Analysis and quasistatic FE modeling of long period impulsive events associated with explosions at Stromboli volcano (Italy)

Markus Kirchdörfer
Institut für Geophysik, Stuttgart, Germany

Abstract
Broadband seismic measurements performed in 1995 and 1996 in the summit region of Stromboli are analyzed. The experiment in 1995 used an array of four Guralp seismometers and one Wielandt-Streckeisen seismometer. The stations were installed around the craters in a semicircle with a radius of about 500 m. This implies that the seismic signals are dominated by near field motions up to frequencies of about 2 Hz. The observed Strombolian explosions are preceded by long-period ground motions occurring between 20 s and 70 s prior to the ejections. They are obviously generated by a slow pressure increase within the magma conduits. The long-period signals are simple compared to the short period wave forms. Four classes of pulse-shaped seismograms can be distinguished. The radiation pattern is radially symmetric with respect to the crater region. Particle motion analysis indicates that the seismic sources are located between 50 and 200 m below the crater terrace. Hydrostatic model sources were studied by means of finite element calculations with different geometries, *i.e.* ellipsoids, in a solid cone modeling the topography of Stromboli. The results suggest that the explosive events on Stromboli originate from a shallow vertically elongated volume source.

Key words *volcano seismology – long-period measurements – Stromboli – finite element calculations – volcano sources*

1. Introduction

In volcano seismology, seismometers with an eigenperiod of 1 s or less have commonly been used. In recent years, several groups of researchers began to use broadband seismometers. The long-period part in the recordings of the seismic signals radiated by volcanic sources is now of special interest.

Mailing address: Mr. Markus Kirchdörfer, Institut für Geophysik, Richard Wagner Straße 44, D-70184 Stuttgart, Germany; e-mail: maki@geophys.uni-stuttgart.de

In the near-field of volcanic sources, *i.e.* the area around the craters, the seismic signals with periods above 1 s are much larger than the source - receiver distance. In this case wave propagation and site effects may be neglected. With seismometers of 120 s eigenperiod and appropriate digital signal restitution it is possible to analyze seismograms up to a period content of about 1000 s.

2. Seismic measurements in a summit array in 1995

Seismic measurements were made in July 1995 using a summit array of four Guralp-seismometers CMG-3T (University of Leeds) and one Wielandt-Streckeisen seismometer STS2 (University of Stuttgart). All seismometers are three-component instruments with an eigenperiod of 120 s.

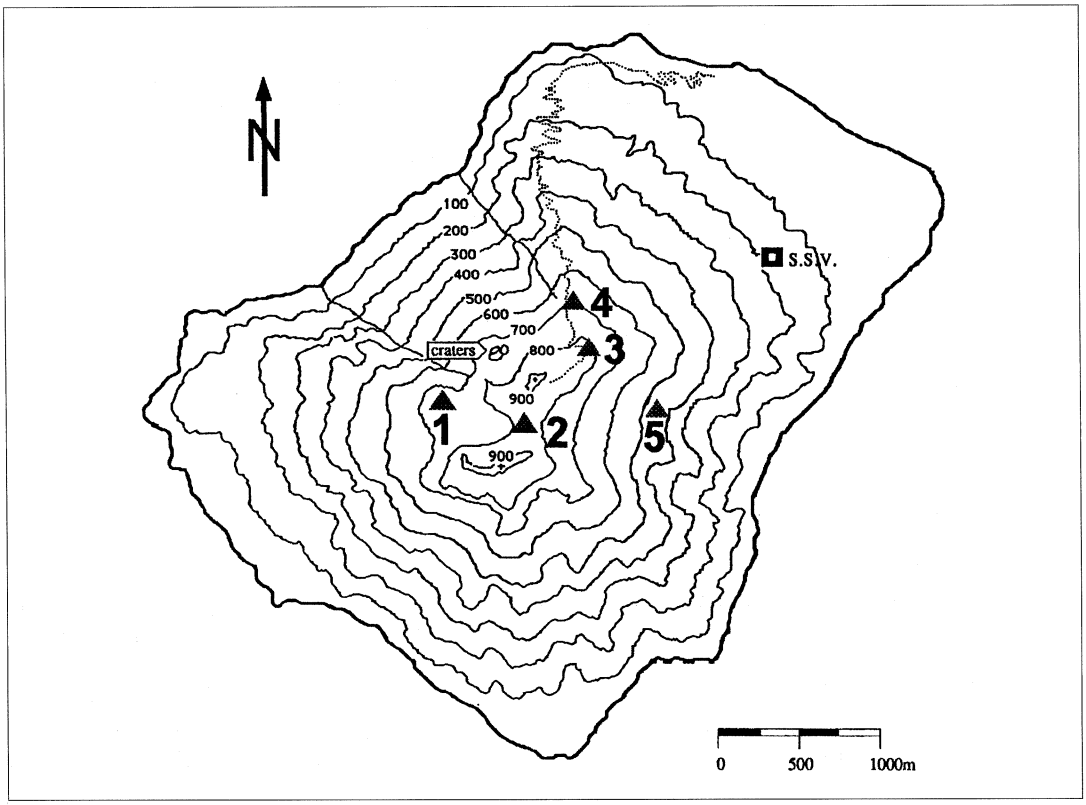

Fig. 1. Sketch map of the island of Stromboli showing the location of the seismic broadband stations. Numbers 1 to 5 indicate Guralp CMG-3T instruments of the University of Leeds. A Wielandt-Streckeisen STS2 seismometer of the University of Stuttgart was installed additionally in station 2. S.S.V.: Semaforo San Vincenzo, Observatory of the University of Florence.

The stations were installed in a semi-circle with a radius of about 500 m around the craters (fig. 1). In station 2 the STS2 and a CMG-3T were buried for a huddle test. A fifth Guralp station was positioned about 1000 m away from the craters.

The data acquisition systems were MARS 88 digital recorders with a dynamic range of 96 dB, operating at a sampling interval of 16 ms.

The data were split into a short-period part (< 1 s) and a long-period part (> 1 s) by filtering. The chosen high pass filter simulated a 1 s seismometer. To derive the long-period data a Butterworth low pass filter of the order 8 was used. A deconvolution was performed in the frequency range by multiplicating the Fourier velocity spectrum of the time series of one hour duration with the inverse of the seismometer's frequency response function. An integration of the restituted time series led to ground displacement.

Although the observed seismic signals lie dominantly within the bandwidth of the seismometer, a deconvolution to a substantially larger period is necessary in order to restore an approximated true waveform of the ground motion. We obtained stable results when deconvolving the seismometer response to periods of 1200 s or even larger. Instabilities occurring as long-period noise were supressed by fitting and subtracting a low-order polynomial.

2.1. *Observations with the vertical components*

All of the observed signals of the Strombolian explosions have pulse-shaped, essentially one-sided waveforms in the period range between 1 s and 1200 s. In general, the vertical components show a slowly increasing upward, *i.e.* compressive, amplitude in their first part, followed by a significant and fast downward, *i.e.* decompressive, motion. The precursor phase lasts typically between 20 s and 70 s before the beginning of the decompressive phase.

Typical ground displacement signals are shown in fig. 2. The following points can be

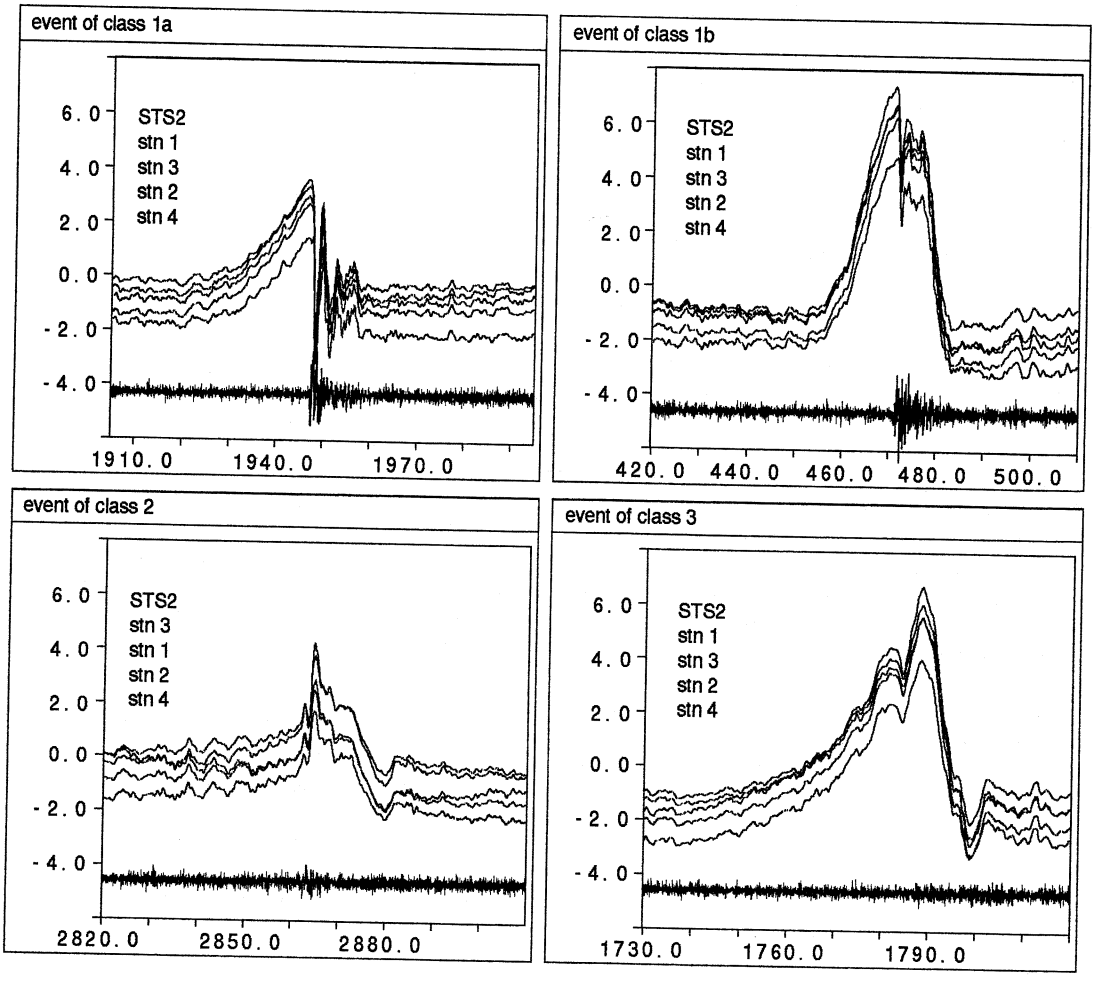

Fig. 2. Typical seismic events representing the four classes as discussed in Section 2.1. The figures show the ground displacement in a period range 1 s - 180 s as recorded with the summit array (stations 1 to 4 and an additional STS2 seismometer at station 2) on July 8, 1995. The time scale is in seconds after 22:00 UT (full scale is 90 s); vertical amplitudes are in micrometers (full scale is 14 μm). The short period signals (bottom trace) are simulated seismograms of a seismometer with 1 s eigenperiod, obtained from the STS2 record by high pass filtering.

emphasized:

1) The seismic events can be divided into four classes. The events of two classes (1a and 1b) could be associated with the Zolfo crater, class 3 events with the Torreone crater by means of visual crater observations. The class 2 events could not be correlated to visible explosive phenomena at the craters.

2) The ground displacement at the five seismometers of the summit array is almost identical in a period band from 1 s up to 1200 s.

3) The overall ground displacements in the long-period range are higher than the ground displacements in the short-period range by a factor of 2 (class 1) up to a factor of 10 (class 3).

4) The onset of the short-period signals (< 1 s) which are associated with explosive volcanic activity typically coincide with the beginning of the decompressive phase. These short-period signals are normally followed within a few seconds by the visible exhaustion of ejecta (Fadeli, 1984).

Of 58 events analysed, 21 were classes 1a and 1b, 15 class 2 and 22 of class 3.

Compared to seismograms which Neuberg and Luckett (1996) recorded in 1992 at a similar distance from the craters, the signals presented here are more clearly one-sided. This is most probably due to the extended long-period bandwidth in this study.

The waveform at station 5 corresponds to that at the other stations. The ground displacement approximates a quadratic decay with increasing radial distance to the crater area.

Cross-correlations of the events show traveltimes of about 0.6 s between station 2 respectively 3 and station 5, indicating a propagation velocity below 1000 m/s.

2.2. *Observations with the horizontal components*

Geographic north was determined using a sun compass to allow a correct orientation of the horizontal components.

A particle motion analysis of the impulsive events shows linearly polarized signals at all the stations (figs. 3 and 4). The radial directions (dotted lines in fig. 4) converge to the crater area. The horizontal signals might be contaminated by tilt (see paper by Wielandt and Forbriger, 1999). However, this affects both components in the same way, so the directional analysis is not disturbed. There is only a marginal difference between the azimuth angles of events belonging to different classes. Even at stations 2 and 3 an identification of the crater actually shooting is not possible by means of the polarization of the long-period ground displacement.

Similar waveforms as those in the vertical seismic traces can be seen in the radial component at each station with an about 4 to 8 times larger amplitude (fig. 5). A signal with a still longer period is superimposed which can be identified as a displacement-associated tilt signal (Wielandt and Forbriger, 1999).

2.3. *Estimation of source depth*

Polarization plots (fig. 6) of the vertical *versus* the radial displacement for 30 s preceding the decompressive phase of an explosive event show similar linearly polarized signals as in the azimuth plane. This analysis indicates that the seismic source is at shallow depth beneath the crater vents. Source depths between some ten meters and 200 m are found. This backward projection of the particle motion is based on a simplistic model of the source and medium. The influence of inhomogeneities and of the topography on the apparent direction of the signal are not yet clear. Sources seem to be estimated too deep principally by this method as model calculations showed (see Section 4). Furthermore, the tilt signal contained in the radial component leads to larger depths because displacement and tilt act in opposite directions on a horizontal seismometer.

The result is in good accordance with Neuberg and Luckett (1996) and Wassermann (1997).

3. Comparison with seismic data recorded in 1996

A second field experiment was performed in September and October 1996. Stations 1 and 2 were sited as in the year before.

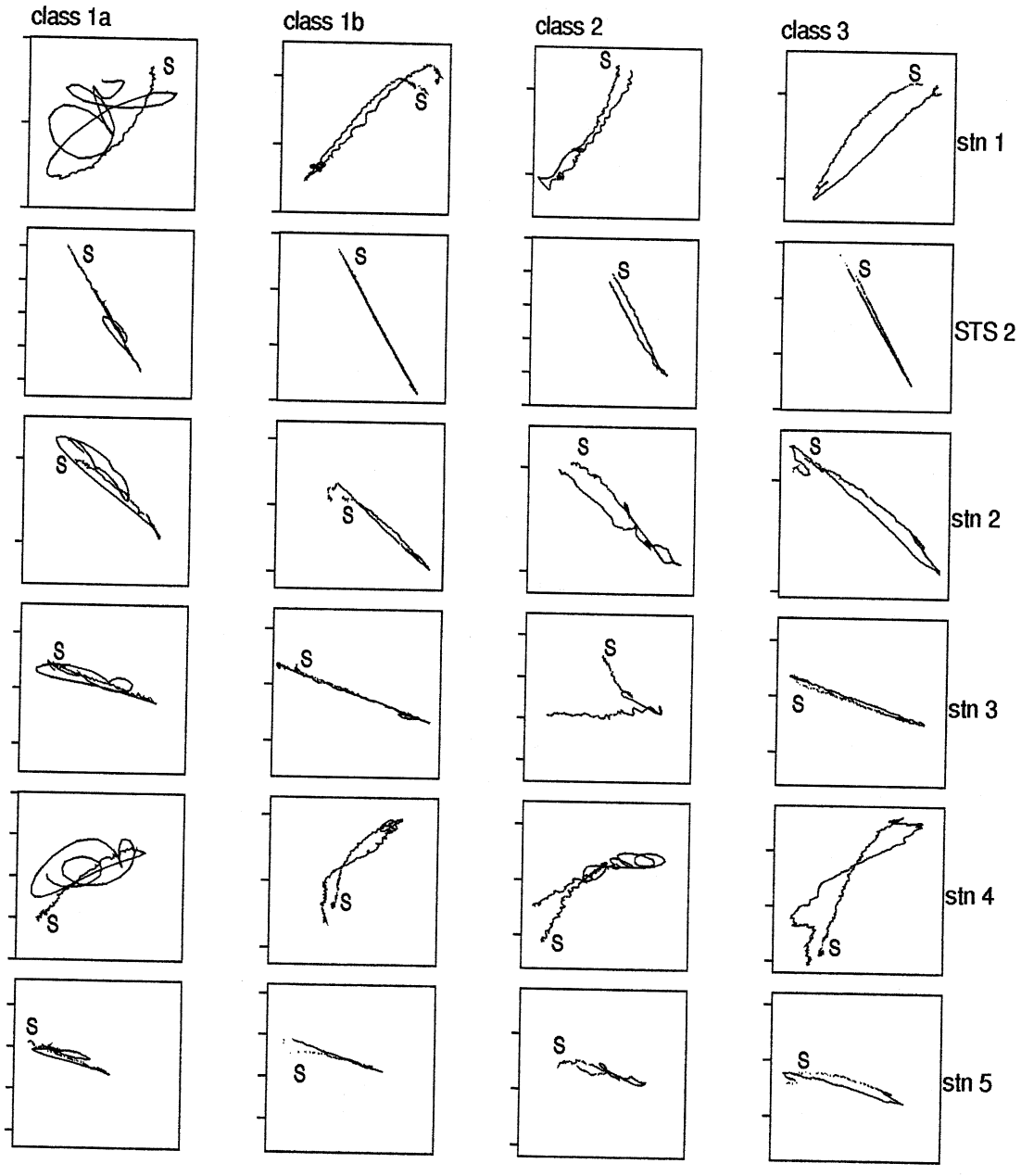

Fig. 3. Particle motion analysis in the azimuth plane. The figure shows four events belonging to different classes (from left to right) recorded at six stations (from top to bottom). The signals are restituted to a period of 120 s. A deconvolution with the seismometer's eigenperiod corresponds to a phase correction. Letter 's' marks the beginning of each trace.

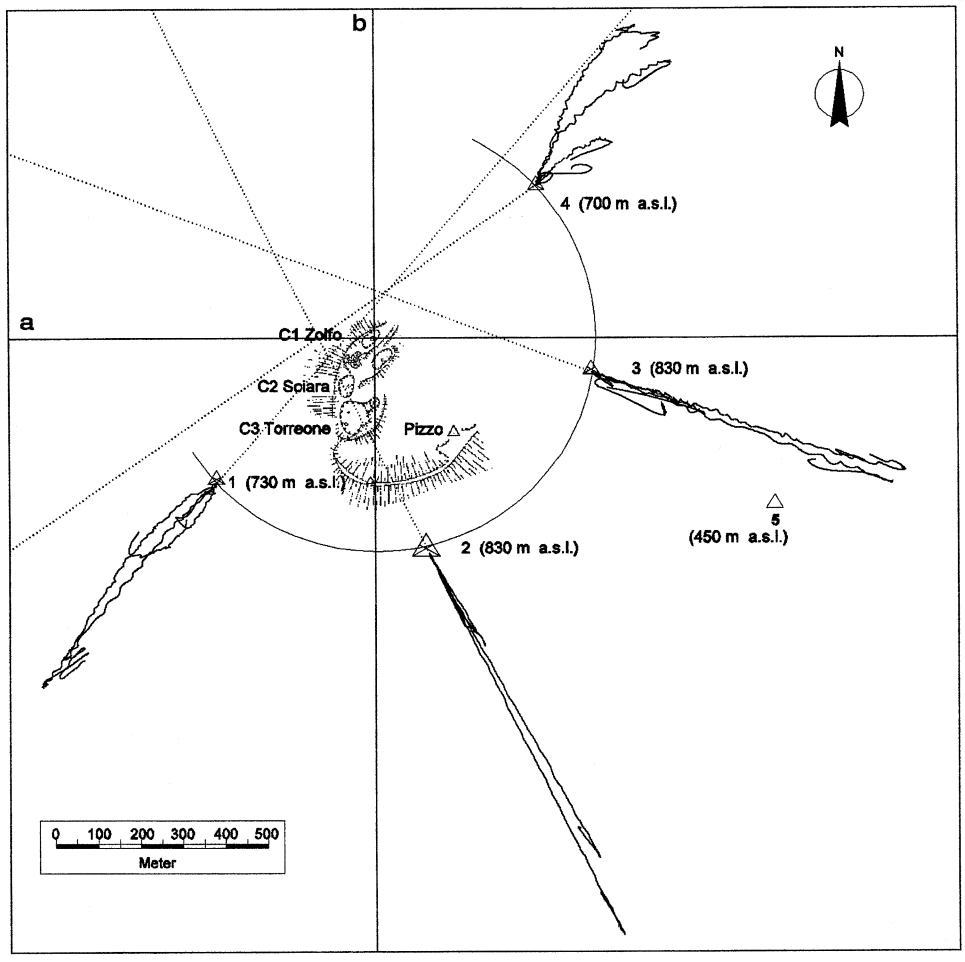

Fig. 4. Sketch map of the crater region with the seismometer sites. At sites 1 to 4 the initial phases of the azimuthal particle motion of the four events shown in fig. 2 are drawn. The dotted lines indicate the directions of the radial component of the ground motion.

In 1996 Stromboli volcano was in a different state. After an episode of very high explosive and dangerous activity in the summer of 1996 (Carniel and Alean, 1996) only very rare visible eruptive activity was observed during the experiment. Unlike the observation period in 1995 a distinction of active craters by eyes was not possible.

The seismic traces were processed as described above. Two waveforms of 1995 could be found again: events of class 2 and class 3 (fig. 2). On an average they occur with double amplitude. The source of the seismic signals seems to be the same as in 1995, since the particle motion analysis at station 2 gives the same azimuth and inclination angles.

About a tenth of the seismic events show a waveform which was not found in 1995 (fig. 7). These pulses show small ground movement in the short-period part.

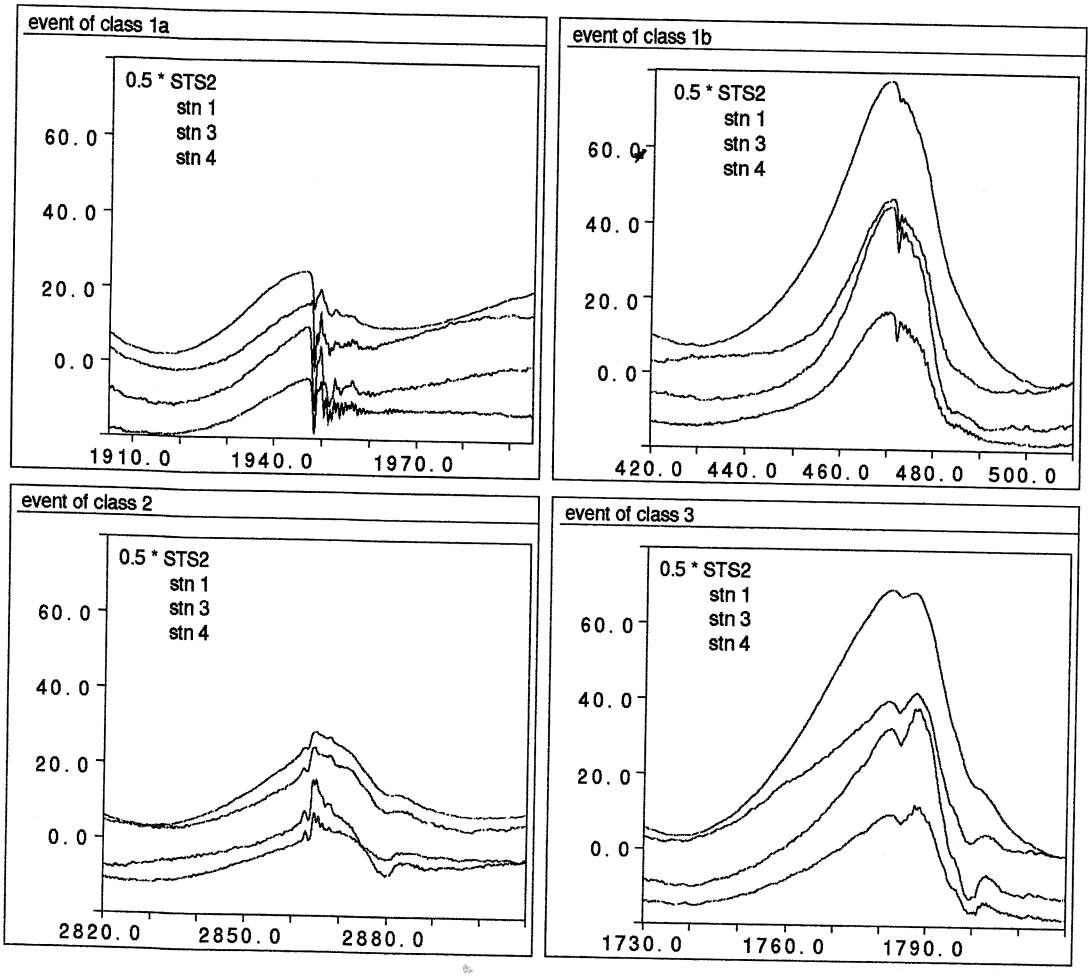

Fig. 5. Comparison of the radial components of the seismic events corresponding to fig. 2. The time scale is in seconds after 22:00 UT on July 8, 1995; amplitudes are in micrometers. The amplitude of the STS2 signal, which is strongly affected by tilt, is reduced by a factor of 2.

4. Comparison of finite element models with Mogi's model

The slow compressive phase of the seismic signal preceeding a Strombolian explosion can be interpreted in terms of a volume source. The Mogi model – *i.e.* a spherical, hydrostatic pressure source at a specified depth in an ideal elastic halfspace; Ishihara (1990), Mogi (1958) – provides a framework for such an interpretation. However, it does not take into account the conical shape of the volcano or topographic details. It was therefore of special interest to compare the predictions of the Mogi model with finite element calculations to obtain more realistic models of a volcano. The commercial software package «Abaqus» of Hibbitt, Karlsson & Sorensen, Inc., running on a NEC SX-4 computer was used for this purpose.

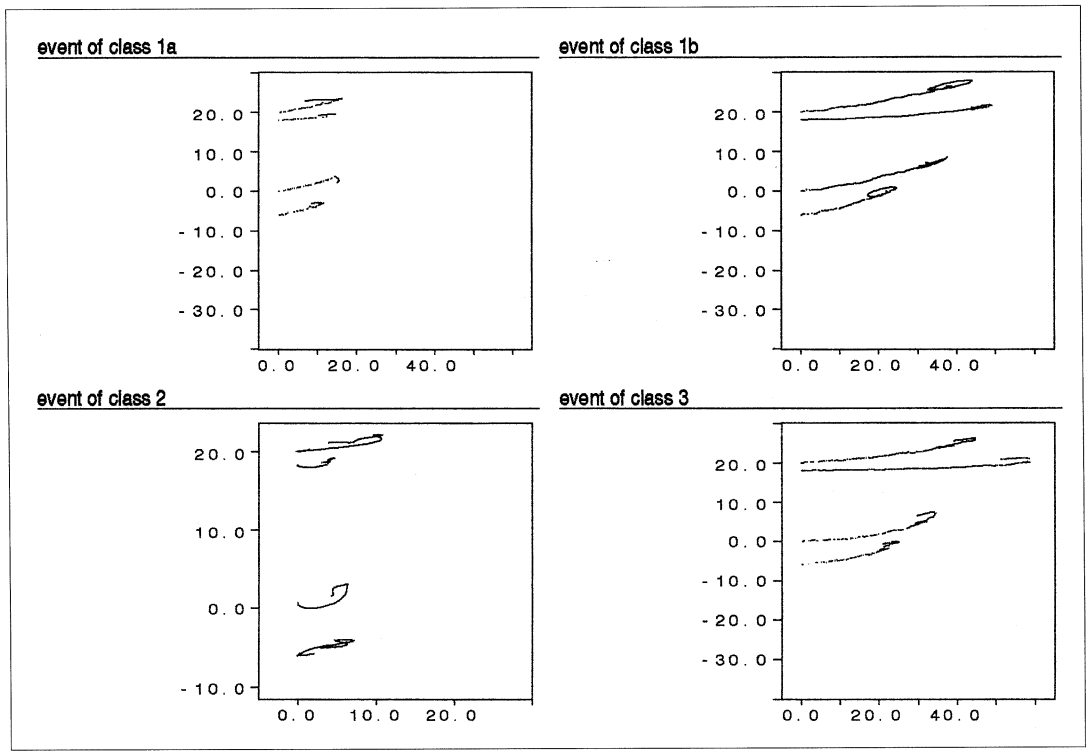

Fig. 6. Comparison of the particle motion in the vertical plane. The time interval is 30 s preceding the explosive decompressive phase of the events shown in fig. 2. In each plot the signals are arranged in the order of the station's elevation above sea level (ref. to fig. 4).

All the models presented here are cylindrically symmetric around the vertical axis. The finite element method was first verified for a Mogi-type model by comparison with the analytical solution. The infinite halfspace was simulated with a mesh whose lateral extent is ten times larger than the largest radial distance of interest and whose depth extent is five times larger than the source depth. At these distances the node displacements are very small compared to those in the vicinity of the source and therefore they can be neglected. It is then justified to fix the nodes at the end of the mesh opposite the symmetry axis and at the bottom layer to give translational stability to the mesh, and to anchor it in the case of loading.

The graphs in fig. 8 compare vertical and radial displacements of the FE-model with the analytical solution of the Mogi-formulae. The radial distances and displacements are measured in a horizontal plane.

The vertical displacement of the Mogi model is

$$u_v = 0.75 \frac{a^3 \cdot \Delta p}{\mu} \frac{D}{(D^2 + r^2)^{3/2}}$$

and the radial displacement along the surface of the halfspace is

$$u_r = 0.75 \frac{a^3 \cdot \Delta p}{\mu} \frac{r}{(D^2 + r^2)^{3/2}} .$$

The parameters for the present calculation are:

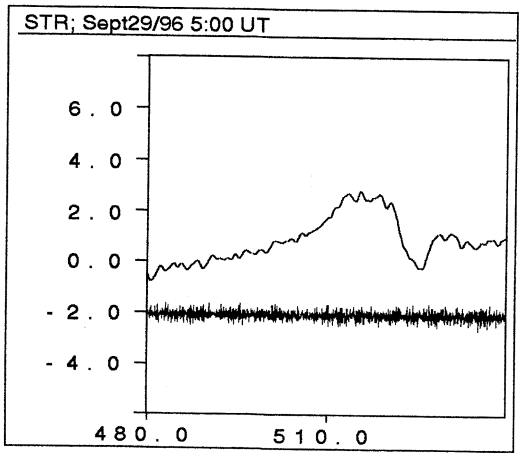

Fig. 7. Comparison of long period *versus* short period record. The example represents the new class of events which occurred in 1996. Time scale is in seconds; vertical amplitude is in micrometers. The short period signal (bottom trace) is a simulated seismogram of a seismometer with 1 s eigenperiod, obtained from the STS2 record by high pass filtering.

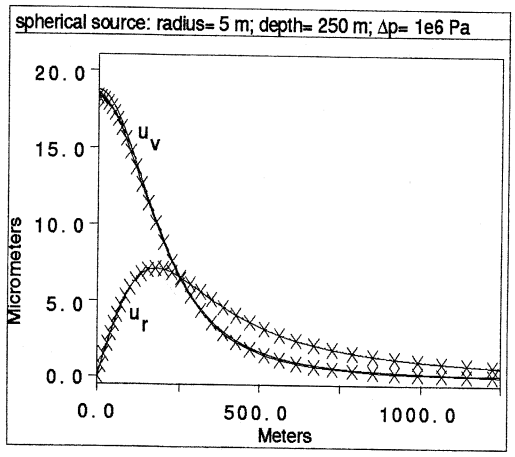

Fig. 8. Comparison of the analytical solution of the Mogi model *versus* the finite element calculation (crosses) of vertical displacement u_v and horizontal displacement u_r along the surface of an elastic halfspace with shear modulus $\mu = 8 \cdot 10^7$ Pa and Poisson's ratio = 0.25.

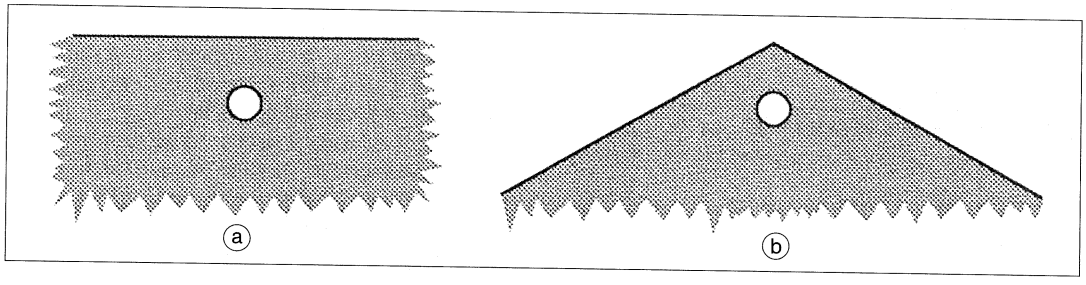

Fig. 9a.b. Sketch of two model configurations studied in the text. a) Spherical source in a halfspace; b) spherical source in a conically shaped solid

source-radius a = 5 m, hydrostatic pressure difference $\Delta p = 10^6$ Pa, source-depth D = 250 m and shear-modulus of the medium $\mu = 8 \cdot 10^7$ Pa. The low value for μ (a figure normally found for clay) may represent the heterogeneity and fissuring of the much harder material building up a volcanic cone. The values were chosen so that the measured vertical displacement of about 2 μm results in a distance to the source of 500 m.

It is obvious from fig. 8 that the finite-element version of the Mogi-model fits the analytical solution very well.

Figure 9a,b show schematically the configurations of the two studied model types: a) a spherical source embedded in a halfspace and b) in a conical solid with a slope of 30°.

The sources in the conical models were positioned shallow below the summit of the cone

and high above the FE-model's base. This is different from the geometry used by Cayol and Cornet (1997) where the source is located deep below the base of a flat cone. Our geometry represents more closely the situation on Stromboli than on Etna as in their work.

For the conical model (surface deformation in fig. 10a and displacement graphs in fig. 10b)

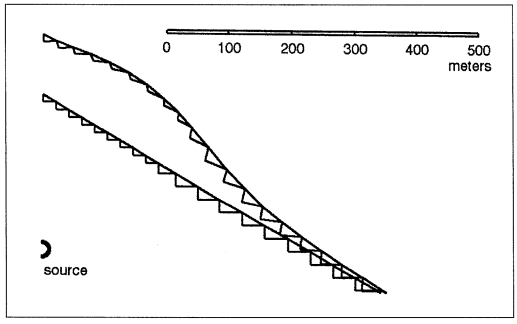

Fig. 10a. Deformed surface over a spherical hydrostatic source in a cone with 30° slope. The source location at a depth of 250 m and the undeformed FE mesh structure are outlined.

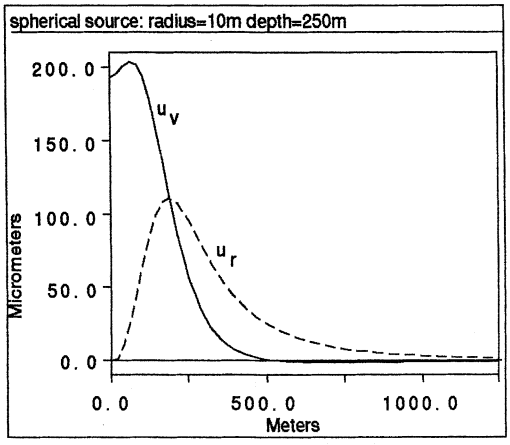

Fig. 10b. Vertical u_v and radial u_r displacement of a spherical source in a cone with 30° slope as sketched in fig. 10a. Source radius = 10 m, source depth is 250 m, pressure rise is 10 bar and shear modulus is $8 \cdot 10^7$ N/m^2; Poisson's ratio = 0.25.

the following results can be summarized:

– The maximum displacements are larger than in the halfspace: the source is less constrained by the surrounding material.

– The maximum vertical displacement does not occur vertically above the source.

– The ratio $\frac{u_r}{u_v}$ is larger than in the Mogi model when $r > D$, and smaller when $r < D$.

– At any distance, the particle motion points away from an apparent source that is below the actual source, *i.e.* the actual source is shallower than the particle motion appears to indicate.

Besides the spherical source, oblate (flattened, figs. 11a,b) and prolate (vertically elongated, figs. 12a,b) ellipsoidal sources in a cone were investigated. Figure 11a, respectively fig. 12a, show the deformed surface in a sectional drawing whereas fig. 11b and fig. 12b show the appropriate radial and vertical displacement.

The model parameters are: source depth: 250 m, $\Delta p = 10^6$ Pa, $\mu = 8 \cdot 10^7$ Pa as chosen for the other models. For both, the aspect ratio of large half-axis to short half-axis is 10:1.

The results with the oblate source do not correspond with the measurements on Stromboli, where the radial displacement at a sufficiently large distance (500 m or more) exceeds the vertical by a factor of up to 10.

The prolate source seems to be more realistic: the horizontal to vertical displacement ratio is much closer to the measured values. The volumes of the sources were chosen in such a way that the vertical displacements are comparable at specific radial distances.

As one might intuitively expect, the largest surface displacements from the spherical source occur in the nearest parts of the conical surface, those from the vertically prolate source below this level, and those from the oblate source above this level up to the summit.

5. Conclusions

Broadband seismograms obtained in the summit region of Stromboli show one-sided impulsive waveforms of which the short-period seismic event is only a minor part. Despite the

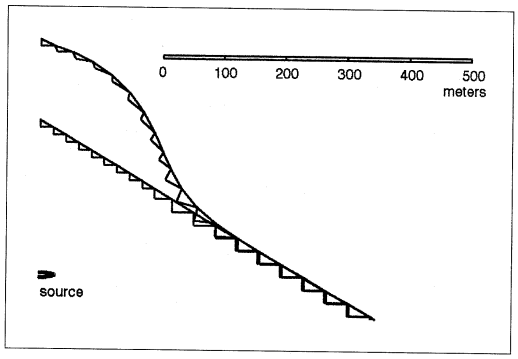

Fig. 11a. Deformed surface over an oblate hydrostatic source in a cone with 30° slope. The source location at a depth of 250 m and the undeformed FE mesh structure are outlined.

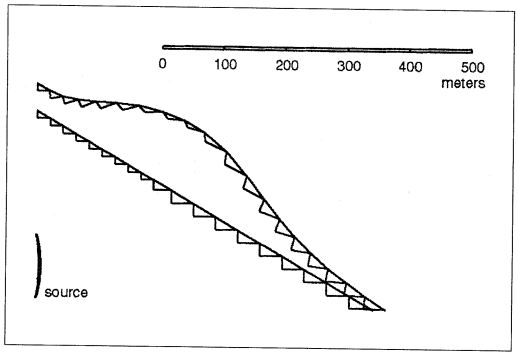

Fig. 12a. Deformed surface over a prolate hydrostatic source in a cone with 30° slope. The source location at a depth of 250 m and the undeformed FE mesh structure are outlined.

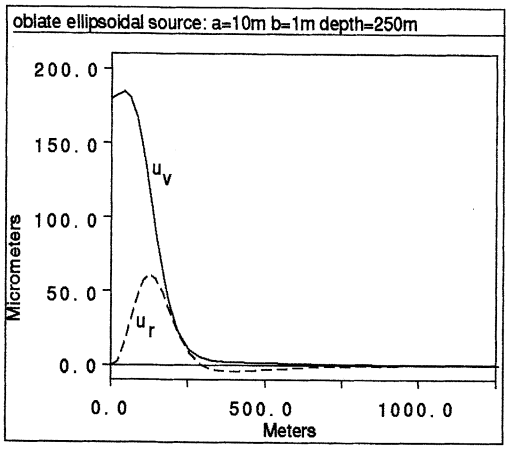

Fig. 11b. Vertical u_v and radial u_r displacement of an oblate source in a cone with 30° slope as sketched in fig. 11a. Horizontal half-axis = 10 m, vertical half-axis = 1 m, source center is at a depth of 250 m, pressure rise is 10 bar and shear modulus is $8 \cdot 10^7$ N/m^2; Poisson's ratio = 0.25.

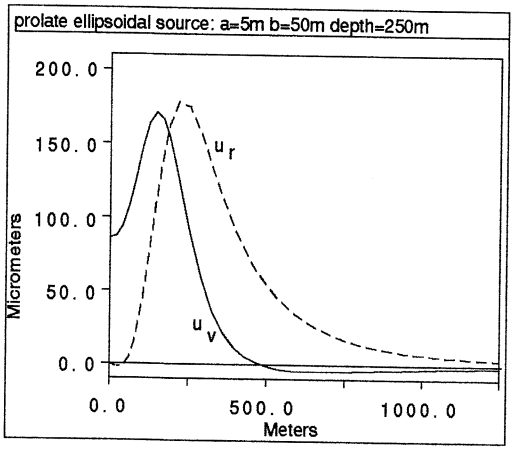

Fig. 12b. Vertical u_v and radial u_r displacement of a prolate source in a cone with 30° slope as sketched in fig. 12a. Horizontal half-axis = 5 m, vertical half-axis = 50 m, source center is at a depth of 250 m, pressure raise is 10 bar and shear modulus is $8 \cdot 10^7$ N/m^2; Poisson's ratio = 0.25.

complicated structure and topography of the volcano, the waveforms at all summit stations are almost identical. We infer that they represent the time history of pressure buildup and release in the volcanic source that controls the explosive activity of Stromboli.

Finite-element models describing a conical volcano show that the long-period seismic displacements observed on Stromboli are likely to originate from a shallow and vertically elongated volume source. This corresponds to the volcanological model of vertically elongated pipes.

Acknowledgements

I am grateful to R. Schick and E. Wielandt who supported this work with in-depth discussions and specific advice. The data used in this study were collected in a field program by the University of Leeds, (U.K.) and the University of Stuttgart (F.R.G.). I thank J. Neuberg and Th. Forbriger for making the data available.

The work was supported by the Deutsche Forschungsgemeinschaft (DFG).

REFERENCES

CARNIEL, R. and J. ALEAN (1996): *STROMBOLI On-Line, Recent and Ongoing Activity of Stromboli and Other Volcanoes,* WWW-Site, http://www.ezinfo.ethz.ch/ezinfo/volcano/seismik/seismike.html

CAYOL, V. and F.H. CORNET (1998): Effects of topography on the interpretation of the deformation field of prominent volcanoes – Application to Etna, *Geophys. Res. Lett.*, **25**, 1979-1982.

FADELI, A. (1984): *A Study on the Eruption Mechanism of Volcano Stromboli (Italy),* Institute of Geophysics, University of Stuttgart, Publication No. 213, 1-71.

ISHIHARA, K. (1990): Pressure sources and induced ground deformation associated with explosive eruptions at an andesitic volcano: Sakurajima volcano, Japan, in *Magma Transport and Storage,* edited by M.P. RYAN (John Wiley & Sons), 335-356.

MOGI, K. (1958): Relations between the eruptions of various volcanoes and the deformations of the ground surfaces around them, *Bull. Earthquake Res. Inst.*, **36**, 99-134

NEUBERG, J. and R. LUCKETT (1996): Seismo-volcanic sources on Stromboli volcano, *Ann. Geofis.,* **39** (2), 377-391.

WASSERMANN, J. (1997): Locating the sources of volcanic explosions and volcanic tremor at Stromboli volcano (Italy) using beam-forming on diffraction hyperboloids, *Phys. Earth Planet. Int.*, **104**, 271-281.

WIELANDT, E. and TH. FORBRIGER (1999): Near-field seismic displacement and tilt associated with the explosive activity of Stromboli, *Ann. Geofis.*, **42** (3), 407-416 (this volume).